Turbine cascade calculations with structured and unstructured meshes

Pénélope LEYLAND [1] Peter OTT [2] Roland RICHTER [3]

Ecole Polytechnique Fédérale de Lausanne, CH-1015 Lausanne

Abstract. Quasi-three-dimensional, inviscid, transonic flows in cambered turbine cascades are calculated using different time and space accurate numerical methods based on either structured finite difference type H-grids or unstructured finite element type ones. The calculations compare well for the overall flow fields. Validation with experimental data shows good agreement. Unsteady calculations are performed using the structured method.

1 Introduction

Numerical investigation of transonic flow in cambered turbine cascades is an important part of the design analysis of gas turbines. The simulation of pitching modes, vibrating modes and flow disturbances contribute to the investigations carried out within experimental set-ups for predicting the unsteady characteristics of the aeroelastic behaviour of modern turbocompressor cascades. As technology advances, the individual parts, such as the blades, in turbomachinery are getting more and more slender as the diameter of the machines becomes smaller, with higher mass and flow speeds. The blade loads due to the unsteady flow and the deformable structure as well as induced aeroelastic phenomena, such as flutter, pitching and forced vibrations are thus becoming more and more important to understand, predict and model correctly.

The cost and difficulty of full unsteady measurements within turbomachines lead to the consideration of cascade experiments and prediction methods to obtain stability limits. CFD is also now an everyday tool for the design engineer, and is used as a prediction and a validation method. With the growth of high performance computing, complete geometry calculations should be feasible within the next decade. However, the underlying numerical methods are just another tool, and as such must be extensively validated on individual parts and generic forms in order to create a viable design methodology along with experimental results. For a realistic geometry viscous effects are far from negligible, especially, for instance, for shock boundary layer interactions at the blades' trailing edges, where pressure losses are important. Whereas for many aeroelastic considerations such as flutter and dynamic loads, as these concern the integrated pressure forces, viscous effects can be modeled by force terms, and inviscid methods are sufficient for calculating margins.

The numerical methods considered in this paper concern only non-viscous flow over linear cascades. The methods use either structured or unstructured meshes. All methods are time and space accurate. Unstructured meshes are particularly suited to simulate unsteady flows over complex geometries because of their capacity and flexibility to dynamically refine and derefine the computational mesh to follow transient and unsteady phenomena. Although the underlying meshes are of finite element type, a finite volume approach can be also used to simulate the flow field and to calculate the aerodynamic forces. Structured meshes have more direct flow field analysis possibilities, which is of primary importance when comparison with particular measurement sites is required, and are often more robust. In particular, unsteady effects such as vibration bending modes are often easier to implement. Coupling such numerical solvers to a structural analysis programme permits the evaluation of aeroelastic constraints within the structure itself.

Two distinct profiles are considered here; one with a relatively high blade thickness and camber operating under high subsonic flow conditions, the other with a less accentuated camber and thickness operating also with subsonic inflow conditions, and transonic exit conditions. The numerical methods employed are a Van-Leer MUSCL flux vector splitting method in space for

[1] Institut de Machines Hydrauliques et Mécanique des Fluides, (IMHEF)
[2] Laboratoire de Thermique Appliquée et de Turbomachines, (LTT)
[3] CRAY Research Inc., PSE

the structured case, and either an Osher approximate Riemann solver or a standard centred scheme with artificial dissipation for stability in the case of unstructured meshes. Both schemes use a time advance by Runge-Kutta integration, which allows also unsteady simulation. The calculations compare well for the overall flow fields; the main differences between the methods which are employed here are the flexibility of choosing the periodicity plane for the unstructured case, which can be chosen almost anywhere apart from the singular line. In the structured mesh case, the periodicity condition of the cascade is imposed via a doubling of the interface periodic cell; whereas in the unstructured case, the interface periodicity condition is taken by a direct *updating*. Unstructured grids are also popular for their adaptation possibilities, and the possibility of dynamically adapting the mesh for transient and unsteady flow. Such techniques also allow local improvement of mesh imperfections; whereas the structured mesh techniques give more flexibility for analysis when imposing unsteady modes of flutter and forced vibration.

2 Governing Equations and Numerical Methods

All numerical methods here are explicit second-order accurate in space and time schemes based on finite volume methods.

The Euler equations are thus written in conservative form for the computational domain $\Omega \times \mathbb{R}^+$ as follows :

$$\begin{cases} \dfrac{\partial W}{\partial t} + \dfrac{\partial F(W)}{\partial x} + \dfrac{\partial G(W)}{\partial y} = 0, \ (x,y,t) \in \Omega \times \mathbb{R}^+ \\ \\ \text{Plus initial, } (t = t_0), \text{ inflow and outflow boundary} \\ \text{conditions for } (x,y,t) \in \ , \ \times \mathbb{R}^+ ; \\ \ , \ = \ , \ in \cup \ , \ out \cup \ , \ wall \end{cases} \tag{1}$$

where

$$W = \begin{pmatrix} \rho \\ \rho u \\ \rho v \\ \rho E \end{pmatrix} ; F = \begin{pmatrix} \rho u \\ \rho u^2 + p \\ \rho uv \\ u(\rho E + p) \end{pmatrix} ; G = \begin{pmatrix} \rho v \\ \rho uv \\ \rho v^2 + p \\ v(\rho E + p) \end{pmatrix}$$

ρ is the density, $(u,\ v)$ are the velocity components, p the pressure, and E total energy. The system is closed by a state equation relating the pressure to the total energy, which for a perfect gas gives :

$$p \ = \ (\kappa - 1) \ (\rho E - \rho \frac{u^2 + v^2}{2})$$

where κ denotes the ratio of specific heats.

2.1 Structured Mesh formulation

The system (1) is mapped from the physical plane (x,y,t) to the computational plane (ξ,η,τ) such that (1) becomes :

$$\frac{\partial W^{'}}{\partial \tau} + \frac{\partial F^{'}(W)}{\partial \xi} + \frac{\partial G^{'}(W)}{\partial \eta} = 0 \tag{2}$$

where

$$F^{'} = D^{-1} \{ \xi_t \ W \ + \xi_x \ F \ + \ \xi_y \ G \}$$

$$G^{'} = D^{-1} \{ \eta_t \ W \ + \eta_x \ F \ + \ \eta_y \ G \}$$

D^{-1} is the usual transformation Jacobian. The unknowns are stored at the cell i,j centres, and the Van Leer flux vector splitting algorithm upwinds the fluxes according to a consistent flux decomposition at the interfaces $(i, j - \frac{1}{2})$, $(i, j + \frac{1}{2})$:

$$\begin{array}{l} F_{i+\frac{1}{2},j} \ \equiv \ \Phi_{F_{i+\frac{1}{2},j}}(W_{i,j}, W_{i+\frac{1}{2},j}) \\ F = F^+_{VL} + F^-_{VL} \\ G = G^+_{VL} + G^-_{VL} \end{array}$$

where $(F,G)^{\pm}$ corresponds to a particular decomposition where the eigenvalues of the corresponding Jacobians $A^{\pm}_{VL}$ remain respectively positive or negative, and where the negative part is zero for supersonic flow in one direction. Φ_F defines the numerical flux function. Second order accuracy is obtained by flux limiting using the MUSCL approach on the non-conservative variables [1, 9].

Time integration for this approach is performed using the same 4 stage Runge-Kutta procedure as for the unstructured case. This type of integration proved to be the most efficient one for the cascade calculations presented here, rather than the original optimal 3 stage scheme following the stability analysis of [16]. Discretizing the system (2) leads to a set of coupled ordinary differential equations for the solution $W^n \equiv W(t = n\Delta t)$ of the form :

$$\frac{W_i^{n+1} - W_i^n}{\Delta t} + M^{-1} R(W_i) \ = \ 0$$

with M = the appropriate mass lumping term; then the Runge-Kutta procedure reads

$$\begin{cases} \overline{W}_i^{(0)} & \stackrel{def}{=} & W_i^n \\ \overline{W}_i^{(k)} & = & \overline{W}_i^{(0)} - \alpha_k \ M^{-1} R \left(\overline{W}_i^{(k-1)} \right) \\ W_i^{n+1} & \stackrel{def}{=} & \overline{W}_i^{(m)} \end{cases} \tag{3}$$

with $k = 1, \cdots, 4, \ \alpha_k = 0.15, \ 0.2, \ 0.5, \ 1.0$.

2.2 Unstructured Mesh formulation

For unstructured meshes, an equivalent finite volume method is obtained by considering the "dual" control

volumes of the underlying P1 Galerkin finite element approximation. They are constructed by taking the barycentres of the contributing triangles to a discretisation node i, as in the Figure (1). The Galerkin finite volume method is based upon the variational form of the equations (1) :

$$\int_\Omega W_t \cdot \varphi d\Omega = -\sum_{j \in k(i)} \int_{\partial \mathcal{C}_{ij}} F(W) \cdot n_{ij} d\sigma - \int_{\partial \mathcal{C}_i \cap \Gamma} F(W) \cdot n_\Gamma d\sigma \tag{4}$$

$\forall \varphi$ in the finite element approximation
$\partial \mathcal{C}_{ij}$ denotes the interface boundary of the dual cell around the node i with respect to a neighbouring node j, (see Figure (1)), and $k(i)$ denotes the triangles k surrounding node i.

The numerical scheme is defined by the numerical flux function $\Phi_{F_{ij}}$ in the direction of the normal n_{ij} to the cell interface between states i and j :

$$\int_{\partial \mathcal{C}_{ij}} F(W) \cdot n_{ij} d\sigma \; = \; \Phi_{F_{ij}}(W_i, W_j)$$

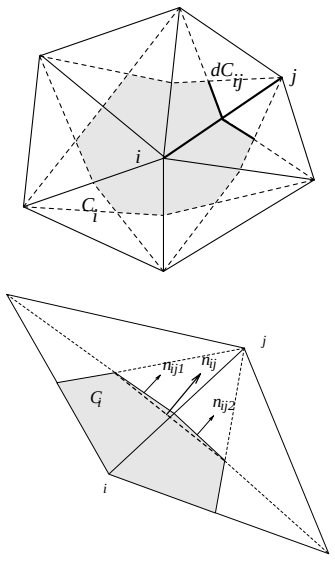

Figure 1: *Construction of dual control volumes on a triangular mesh,* (top)*, illustrating the flux evaluation across the interface,* (bottom).

Here, two such numerical fluxes were considered; a standard centred difference flux with additional fourth- and second-order artificial dissipation for stability and shock capturing respectively, (Jameson type scheme), and the Osher flux which is an approximate Riemann solver. For low subsonic flows, the Osher flux proved more robust, at a higher cost. One of the reasons for the problems with the centred scheme comes from the non-adaptation of the artificial dissipation for subsonic flows [7] where an upwind biasing in the subsonic direction needs to be implemented. The leading edge resolution is more accurate with the Osher solver, and this greatly influences the behaviour on the suction side, where the instability due to the non-adapted dissipation of the centred scheme is strong.

The Osher flux can be written formally as

$$\Phi(W_i, W_j) = \frac{1}{2}\left[F_{ij}(W_i) + F_{ij}(W_j) - \int_{W_i}^{W_j} |A_{ij}(W)| dW \right]$$

where the integral depends on the choice of integration path , between the left and right states at the interface of the cell between nodes i and j. This path is a combination of two compression waves for the truely non-linear fields and a contact discontinuity for the linearly degenerate field. Second-order accuracy is obtained by a third-order MUSCL extrapolation which renders an overall second-order accuracy for irregular meshes with a minmod limiter near discontinuities.

As for the structured method, second-order time integration is assured via a 4 stage Runge-Kutta procedure (3), with coefficients $\alpha_k = 0.25,\ 0.33,\ 0.5,\ 1.0$ for the centred scheme, and a modified one stage procedure for the upwind Osher scheme, [15].

2.3 Mesh optimisation

The unstructured meshes considered here were first generated by an H-mesh generator of Carstens, [5], for a periodic blade-to-blade configuration, with periodicity imposed along the singular line. The original grid was then divided into triangles. This can produce badly oriented cells in the vicinity of the singular line for the unstructured case, where an original C-type generation would have been preferable. The structured mesh methods all used H-grid generation. In general, C - grids for such cambered blade cascades are more complex to generate, and can necessitate CAD tools. This can lead to a lack of regularity within the leading edge zone for the structured mesh. Also, whereas the unstructured methods have greater flexibility for the choice of cascade periodicity plane, most structured mesh difference methods require periodicity along the profile's chord. For complete geometries, it can often be difficult to couple C - grids afterwards with the remainder of the turbo-compressor parts, [11].

The advantages of unstructured grids are also their relative freedom for adapting the mesh via refinement and derefinement of critical zones, [12, 14]. Optimisation of the mesh quality is also integrated into such methods, by structural and geometrical changes. The adaption sensors filter out critical zones such as the shock waves and expansion fans, and then additional nodes can be added in such regions. For the cascades studied here, the most crucial regions are the leading and trailing edges. Insufficient definition and poor quality of cells within these regions will lead to numeri-

cal instabilities that falsify the eventual shock position, and pressure losses along the blade. Once again, it is thus preferable, for an unstructured mesh, to generate the initial grid over the *whole* profile rather than along the singular line, as then further optimisation of the cells around the leading edge is possible. All the results presented in this paper employ meshes with an equivalent number of discretisation nodes and cells.

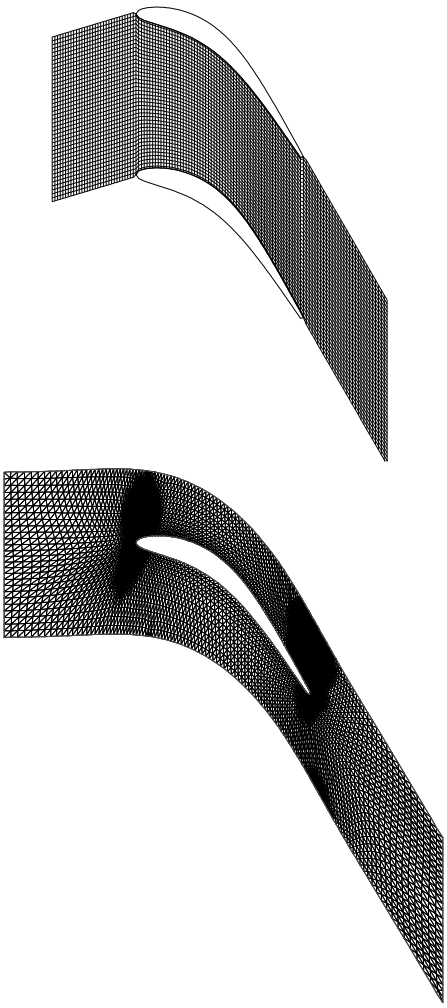

Figure 2: *Structured and Unstructured mesh for the Industrial Gas Turbine cascade studied in this paper.*

3 Boundary Conditions

3.1 Inflow

The structured method takes into account the inlet boundary condition using the methods of "capacitive inlet"; the total pressure and flow angle are imposed and the flow variables are evaluated using a method of characteristics, using Riemann invariants depending on the eigenvalues. In the unstructured method, boundary conditions are taken into account as a numerical boundary flux, (4), which is solved iteratively using a Riemann solver with the state W_∞ defined by the inlet conditions.

3.2 Outflow

At the outflow boundary, the static pressure is imposed and the same techniques are applied as for the inflow boundary. However, now the state W_∞ in the flux boundary condition must be modified in order to verify the 3 Riemann invariants corresponding to the eigenvalue $U - a$, where U is the normal speed $\vec{u} \cdot \vec{n_{ij}}$ and a is the speed of sound :

$$\phi_1^1 = U + \frac{2}{\kappa - 1} a, \quad \phi_1^2 = \frac{p}{\rho^\kappa}, \quad \phi_1^3 = V$$

and V is the tangential speed. The new values of the state W_∞^* are

$$p_\infty^* = p_{\text{imposed}} \qquad u_\infty^* = u + \frac{2}{\kappa-1}\left(a - \sqrt{\frac{\kappa p_\infty^*}{\rho_\infty^*}}\right)$$

$$\rho_\infty^* = \rho \left(\frac{p_\infty^*}{p}\right)^{\frac{1}{\kappa}} \qquad \rho E_\infty^* = \frac{p_\infty^*}{\kappa-1} + \frac{\rho_\infty^* (u_\infty^*)^2}{2}$$

where $p_\infty^* = \beta\, p_\infty \left(1 + \frac{\kappa-1}{2} M^2\right)^{\frac{\kappa}{\kappa-1}}$, and β is the ratio $\frac{\text{outflow static pressure}}{\text{inflow total pressure}}$.

3.3 Periodic

Unstructured methods allow greater flexibility in the choice of the the cascade periodicity plane which can be chosen almost anywhere apart from the singular line. In the structured mesh case, the periodicity condition of the cascade is imposed here via a doubling of the interface periodic cells; whereas in the unstructured case, the interface periodicity condition is taken by a direct node to node *updating*, as in domain partitioning algorithms, [8]. In this way, the cascade can be represented by a single complete profile between an upper and lower profiles for limiting the domain. If a similar configuration is considered in the structured case, it would be necessary to have a minimum of 3 blades. In figures (5) several planes have been compared.

4 Results

4.1 Subsonic Steady Flow over a Cambered Linear Cascade

A highly cambered relatively thick cascade has been documented in [3] for a variety of conditions. A steady flow simulation has been performed here for a completely subsonic flow with inlet Mach number of .28

Figure 3: *Geometrical set-up of the subsonic linear cascade, $\gamma = 56.6°$ denotes the chordal stagger angle from axial direction, $\tau = .76$ is the dimensionless gap to chord (c) ratio.*

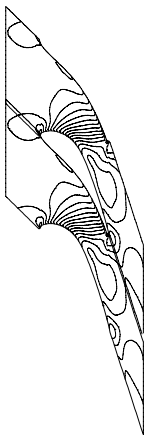

Figure 4: *Inflow Mach number = .28, Local Iso-Mach number contours of the solution obtained with structured mesh with periodicity via cell doubling.*

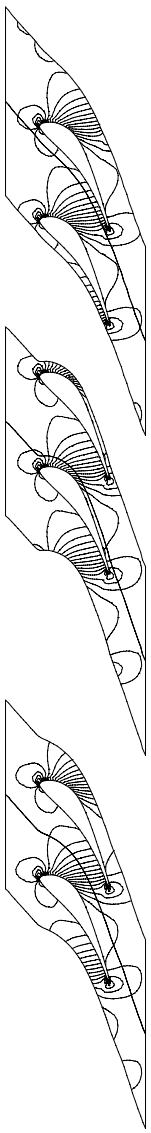

Figure 5: *Inflow Mach number= .28, : Local iso-Mach number contours of the solutions obtained with the unstructured mesh method with different periodicity planes.*

4.2 Subsonic/Transonic Flow over an Industrial Gas Turbine Cascade

A second cascade geometry was considered corresponding to a test case for ABB, for which recent experimental results have been obtained for both steady and unsteady flows in the annular test facility of LTT, [2, 4]. In this case, the profiles are slender, with a lower camber; they produce a transonic acceleration. The flow conditions correspond to a inflow Mach number of 0.32, at an flow angle of 16.7°. Outflow conditions are imposed by fixing the outflow total pressure ratio to .543, which

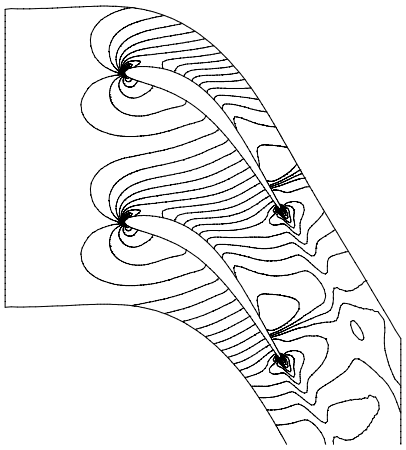

Figure 7: *Local Mach number isolines for the LTT method (*top*), the Denton programme (*centre*), and the IMHEF method (*bottom*).*

Figure 6: *The Industrial Gas Turbine Blade Configuration.*

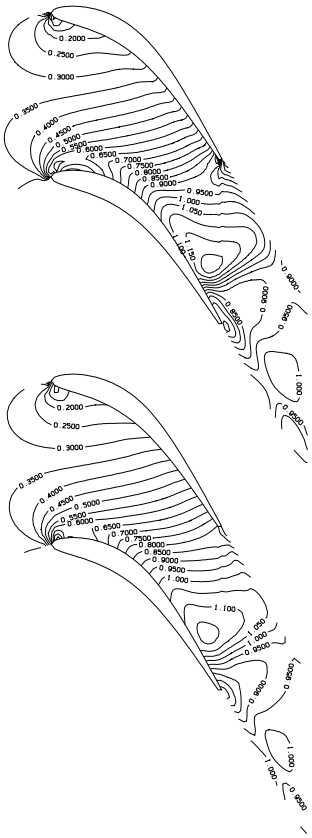

For the unstructured method, both solvers were tested. The centred scheme with second-and fourth- order dissipation captured well the transonic shock near the trailing edge on the suction side, however due to excessive entropy production at the leading/trailing edges, (due partly also to the quality of the triangles/cells in these zones), the isentropic Mach number and pressure coefficient profiles along the blades are influenced by the corresponding solution field overshoots. The approximate Riemann solver of Osher gave more stable results, and maintains the mathematical entropy condition, [14]. The steady state solutions obtained by both the structured (LTT) and unstructured (IMHEF) methods gave similar solutions as shown in the figures (7). The solution has been artificially doubled for the unstructured case for easier comparison.

The quantitative comparisons shown here present the isentropic Mach number and the pressure coefficient along the profiles for the pressure and suction sides, where

$$M^2_{isentropic} = \frac{2}{\kappa - 1}\left\{\left(\frac{p^{in}_{total}}{p^{local}_{static}}\right)^{\frac{\kappa-1}{\kappa}} - 1\right\}$$

and

$$C_p = \frac{p^{local}_{static} - p^{in}_{static}}{p^{in}_{total} - p^{in}_{static}}$$

for the methods mentioned above, as well as a programme of Denton (used in its inviscid mode) on the fine structured grid, [6], (Figures (8)). For the isentropic Mach number profiles, the structured methods capture the shock on the suction side as long as the grid is fine enough, whereas the unstructured method does not show such grid dependency. Only comparisons for the (fine) grids mentioned above are thus given.

bility limits of the cascade. In order to study bending effects, the cascade is allowed to vibrate at frequencies determined by the experimental set-up, and prescribed by the constructor. Once a steady-state solution is obtained, (after approximately 5000 global iterations in time), the blades can be put into an unsteady bending mode. Although both methods, IMHEF and LTT are time accurate, only the LTT method allows the calculation of the unsteady bending modes at the moment. The IMHEF method allows single blade pitching calculations by a change of reference frame, [13], but a complete periodic cascade in bending or pitching mode requires the mesh *and* geometry to be moved simultaneously according to the imposed reduced frequency. This technique is more straightforward with the structured mesh method, whereby a certain number of grid points are fixed per station blade to blade in the horizontal direction x, and a new mesh is re-drawn per station, with a straightforward calculation of the unsteady fluxes (F, G) per cycle.

The cascade is forced into a vibrating mode of frequency of $210Hz$, with an interblade phase angle of 180^o and a bending amplitude of $h = 0.4mm$ with respect to the chord length c. For an interblade phase angle of 180^o (the blades move in counter phase) 2 complete blade channels are computed. An interblade phase angle of 90^o would require 4 blade channels. For the unsteady case the periodicity is enforced between the first line of the first blade channel and the last line of mesh points of the last blade channel. The number of time steps needed to fulfill one complete vibration cycle can be computed by taking into account the vibration frequency and the time increment per time step (determined by the CFL condition). After two vibration periods, a periodic flow is established, and over one period the unsteady $\tilde{C_p}$ (amplitude of the first harmonic) and phase can be evaluated.

$$\tilde{C_p} = \frac{1}{h} \frac{p^n_{static} - p^{n=0}_{static}}{p^{in}_{total} - p^{in}_{static}}$$

where $n = n\,\Delta t$.
The results are shown in Figure (9). The agreement with the experimental results is very satisfactory. The influence of the oscillating normal shock on the suction side at about 80% of the chord length can clearly be seen. The discrepancies are due first to the perturbations introduced by the mesh quality at the leading/trailing edges which are enhanced in an oscillating mode, and secondly to the fact that the pressure losses due to viscous effects are not taken into account by an inviscid model.

Figure 8: top: *Isentropic Mach number profiles along the blades for numerical results with the fine grids compared to experimental results;* bottom: *Steady state C_p profiles for the different methods compared to measurements.*

5 Flow through a Vibrating Cascade

Knowledge of the pitching and bending modes is important in obtaining the margins of the aeroelastic sta-

Figure 9: *Unsteady Cp (LTT) versus measurements*

6 Conclusions

Both structured and unstructured mesh solvers have been tested for inviscid flows within linear cascades and the advantages and disadvantages of each method were discussed. The general agreement is close. The relative cost is also comparable. The unstructured mesh solvers have more flexibility for adapting the mesh, which allows accurate discontinuity capturing, and greater freedom for domain decomposition partitioning, which is advantageous for parallel computations. Unstructured meshes are also simpler to generate for complex geometries, as less initial regularity is required, and they have greater flexibility for angular domains. They also possess an interesting potential for calculating high precision unsteady flows. The structured mesh solvers are less memory consuming, and the extraction and analysis of the data are more direct, and allow more straightforward analysis with respect to experimental measurements. For the unsteady calculations considered here, the bending vibrational modes, where it is necessary to move the actual geometry of the blades, structured methods have a distinct advantage to be able to install the vibrational motion, and to analyse the flow at particular times. However, these methods require more constraints for partitioning as for the choice of periodic planes, due to less flexibility of the data structure.

Acknowledgements

The measurements presented here and the development of the method 'LTT' were part of a research project funded by ASEA Brown Boveri, Baden, Switzerland (under the supervision of Dr. K. Vogeler) with financial support from the Swiss government. The work undertaken with the method 'IMHEF' was partly supported by a Swiss government OFES/CEE contract. This support and the authorization to publish the results is kindly acknowledged.

References

[1] Anderson, W.K., Thomas, J.L., Van Leer, B. *A Comparison of Finite Volume Flux Vector Splittings for Flows with Shock Waves.* AIAA 87-1152, 1987.

[2] Bölcs A. *Annular Cascade Test Facility* ASME paper 83-GT-84, 1983.

[3] Bölcs, A., Fransson, T.H. *Aeroelasticity in Turbomachines; Comparison of Theoretical and Experimental Cascade Results.* Communication du laboratoire de Thermique Appliquée et de turbomachines, No.13. Lausanne, EPFL, 1986.

[4] Bölcs, A., Ott, P., Schläfli, D. Interner Bericht LTT-88-25 EPFL, 1988.

[5] Carstens, V. *Transonic Unsteady Aerodynamics and Aeroelasticity.* 73rd meeting of the AGARD Structures and Materials Panel, San Diego, california, 7-11 October, 1991.

[6] Denton, J.D. *The Use of a Distributed Body Force to Simulate Viscous Effects in 3D Flow Calculations.* ASME paper 86-GT-144, 1988.

[7] Jameson A. *Artificial Diffusion, Upwind Biasing, Limiters and their Effect on Accuracy and Multigrid Convergence in Transonic and Hypersonic Flows.* AIAA-93-3359, 1993.

[8] Leyland, P. Bomholt, L. *A Comparison of Data-Parallel and Domain-Decomposition Implementations of Finite Element Codes for CFD on Parallel Architectures.* Proc. Parallel CFD'93, Paris, 1993.

[9] Ott, P. *Oszillierender senkrechter Verdichtungsstoß in einer ebenen Düse.* Ph.D. Thesis, EPFL, 1991.

[10] Ott, P., Bölcs, A., Fransson, T.H. *Experimental and Numerical Study of the Time Dependent Pressure Response of a Shock-Wave Oscillating in a Nozzle.* ASME 93-GT-139, 1993.

[11] Reymond J.-D., Sottas G. *An Osculatory Algebraic Method for the Generation of Meshes in Three-Dimensional Domains of Arbitrary Complexity.* 4th International Conference on Numerical Grid Generation in Computational Fluid Dynamics and Related Fields, Swansea, 1994.

[12] Richter, R. *Schémas de capture de discontinuités en maillage non-structuré avec adaptation dynamique.* PhD Thesis, EPFL, 1993.

[13] Richter, R., Leyland, P. *Precise Pitching Airfoil Computations by use of Dynamic Unstructured Meshes.* AIAA paper 93-2971, 1993.

[14] Richter, R., Leyland, P. *Unsteady Aerodynamics with Non-Hierarchical Auto-Adaptive Dynamic Finite Element Type Meshes.* Paper to appear IJNME, 1994.

[15] Shu, C.H., Osher, S. *Efficient Implementation of Essentially Non-Oscillatory Shock-Capturing Schemes I.* Journal of Computational Physics, No. **77**, p. 439-471, 1988.

[16] Turkel, E., Van Leer, B. *Flux Vector Splitting and Runge-Kutta Methods for the Euler Equations.* Report ICASE 84-27, 1984.